Journal Homepage: http://ijcpe.uobaghdad.edu.iq
Iraqi Journal of Chemical and Petroleum Engineering
Vol. 27 No. 2 (June 2026) 1 – 17
EISSN: 2618-0707, PISSN: 1997-4884

Treatment of real petroleum refinery wastewater using SiO_2/TiO_2 nanocomposite induced by UV–visible light

Sarmad A. Rashid [a, *], Wadood T. Mohammed [a], Harouadi Zine Eddine [b]

a Department of Chemical Engineering, College of Engineering, University of Baghdad, Baghdad 10001, Iraq
b Hydrocarbon and Petrochemical Process Department/ Faculty of Engineering/ University of Pannonia / Veszprém, 8200, Hungry

Abstract

Petroleum refinery wastewater (PRW) is becoming a big problem for both people and the environment, so researchers have been trying harder to find better ways to treat it. One option that looks really promising is using advanced oxidation processes (AOPs) to break down all the pollutants inside this wastewater. In this study, new-designed photoreactor was used to conduct a photocatalysis approach that aimed to remove the chemical oxygen demand (COD) from PRW collected from Al-Diwaniya refinery in the south of Iraq. The geometrically optimized photoreactor enhances the formation of the free radicals required for efficient degradation by maximizing mass transfer and light dispersion. Bare TiO_2 and SiO_2/TiO_2 were fabricated as photocatalysts with the sol-gel technique and then examined by the XRD, FTIR, FESEM, AFM, BET, UV-DRS, and PL analysis. Results showed that, the optimal SiO_2/TiO_2 ratio was 5/95% (S-5) achieving 90% COD reduction efficiency with a photocatalyst dosage of 2 g/L, a reaction time of about 4 h, and using 8 UV-C lamps (8 W each). Under these conditions the process consumed 0.512 kWh/L electricity energy (EE/O). The results demonstrated that COD reduction exhibits behavior consistent with pseudo first order kinetics. In addition, the scavenger experiments revealed that the COD was primarily degraded by the $\bullet O_2^-$ radical. After five cycles, the photocatalyst S-5 maintained its stability and continued to remove over 82% of the COD. Refinery effluent was significantly better treated after using this innovative reactor design in conjunction with the SiO_2/TiO_2 photocatalyst. It provides an ecological, more efficient, and less expensive way to lower COD in PRW.

Keywords: COD reduction; SiO_2/TiO_2 nanocomposite; photocatalytic degradation; PRW; scavenger.

Received on 15/12/2025, Received in Revised Form on 27/02/2026, Accepted on 28/02/2026, Published on 30/06/2026

https://doi.org/10.31699/IJCPE.2026.2.1

1- Introduction

Water is the most important molecule for all known life since it keeps ecosystems alive on Earth and helps various biological processes. The rapid rise of the population these days is primarily due to more automation and economic growth, which makes people more productive and helps countries handle larger numbers of people [1]. Petroleum companies and refineries play an essential role in supporting energy security, improving industrial productivity, and contributing to national economic growth; however, their operations are often associated with significant environmental concerns due to the formation of complicated wastewater streams. However, due to the huge water requirements of the refining process, petroleum refineries produce enormous volumes of complicated effluents. Heavy metals, ammonia, suspended particles, oils, greases, and other chemical additives are among the many organic and inorganic contaminants found in these wastewaters [2]. Due to the huge amounts of petroleum refinery wastewater (PRW) produced (roughly 1.6 times more than the crude oil being processed), treating that wastewater in Iraq presents very hard set of challenges. In addition, it is extremely harmful due to the toxins it contains, which include aliphatic and aromatic hydrocarbons, phenols, carcinogenic substances, and more [3]. Reuse and environmental protection both necessitate appropriate treatment techniques of these effluents due to their complexity and danger [4].

Refinery and industrial contaminated water have been treated using a variety of techniques over the years, including biological treatments [5], membrane filtration [6], forward and reverse osmosis) [7], chemical oxidation, adsorption [8], ion exchange [9], electrocoagulation [10], extraction [11], and flotation [12]. However, there are drawbacks to each approach, such as inefficient removal of trace contaminants [13], long reaction times (particularly in biological applying), and the formation of secondary wastes. Many of the conventional techniques fail miserably when treated tiny or long-lasting contaminants, particularly those that are harmful. Since many physical and chemical methods just transfer contaminants from one phase to another rather than eliminating them, they increase the amount of waste that needs to be handled and may even generate new environmental pollutants [14].

Advanced oxidation processes (AOPs) are a group of chemical treatment approaches that are being used more

*Corresponding Author: Email: sermed.rashid@coeng.uobaghdad.edu.iq

and more in wastewater treatment to eliminate both organic and inorganic pollutants. These processes depend on producing very reactive hydroxyl radicals (•OH) inside the system. These radicals act like strong, non-selective oxidants that attack a wide range of pollutants, breaking them down into smaller and simpler inorganic products [15]. AOPs rely on different oxidants (ozone, H_2O_2, superoxide oxygen, $•O_2^-$), energy sources (sunlight, UV, visible light), and catalysts (like TiO_2 in photocatalysis) to generate these radicals. This big family of processes includes ozonation, Fenton and electro-Fenton, hydrogen peroxide activation, and photocatalysis [16]. The choice and combination of chemicals and energy sources are usually optimized to boost the creation of •OH radicals and achieve better pollutant removal. Photocatalysis in particular has become a promising, eco-friendly, and relatively low-cost method for wastewater treatment [17].

Photocatalysis is distinguished by its use of sunlight or UV light to activate semiconductor photocatalysts such as titanium dioxide (TiO_2). The charge carriers engage in redox processes that produce hydroxyl radicals and superoxide anions ($•O_2^-$), both of which facilitate the degradation of organic contaminants [18]. Photocatalytic treatment is distinguished by its operation at moderate temperatures and pressures, absence of dangerous byproducts, and possibility for "zero" waste compliance, rendering it optimal for sustainable water management [19]. The process commences when the photocatalyst absorbs a photon, resulting in the generation of an electron/positive hole (e^-/h^+) pair [20], as illustrated in Eq. 1:

$$Photocatalyst + h\nu \rightarrow e^- + h^+ \quad (1)$$

Here, $h\nu$ refers to photon energy, e^- is an existence electron, and h^+ is the hole. An important part of photocatalytic oxidation is the formation of hydroxyl radicals (•OH) by means of water oxidation using photogenerated positive holes. These radicals serve as the foundation for the decomposition of organic contaminants on catalyst surfaces [20]. Eq. 2 usually characterizes this process:

$$H_2O + h^+ \rightarrow {}^{\bullet}OH + H^+ \quad (2)$$

When oxygen molecules dissolved in a photocatalytic system interact with photogenerated electrons (e^-), superoxide radicals ($•O_2^-$) are produced. A molecular oxygen atom is reduced by one electron in this interaction, creating an anion of the superoxide radical [21]. This step is typically described by the reaction represented in Eq. 3:

$$e^- + O_2 \rightarrow {}^{\bullet}O^- \quad (3)$$

Heterogeneous photocatalysis is considered an effective and promising approach for water treatment due to its numerous advantages, including complete mineralization of organic pollutants, operation under mild conditions, and minimal secondary waste generation, instead of just moving the pollution from one phase to another like many traditional treatments do. This method also works under normal room conditions, uses catalysts such as titanium dioxide that are reusable, stable, cheap, and not toxic, and requires very little chemical additives [22].

Semiconductors are often used as photocatalysts for treating water. Out of all semiconductor materials, titanium dioxide (TiO_2) is one of the most studied and most used in photocatalysis. This is because of its strong photocatalytic activity, very good chemical stability, being non-toxic, and its ability to break down organic pollutants efficiently when exposed to UV light. Its advantages include high catalytic activity, suitable energy band potential, excellent photochemical stability, and versatility in both acidic and basic environments. TiO_2 is also cost-effective and environmentally friendly, making it suitable for large-scale applications [23]. Bare TiO_2 has a few drawbacks, though, its efficiency in natural sunlight is limited because of its wide band gap, which is roughly 3.2 eV, and limits activation to the UV range. Photogenerated electrons and holes in TiO_2 structure recombine quickly, thus decreasing the material's photocatalytic effectiveness. There are several other issues, such as a small surface area, difficulty in recovering used catalysts, nanoparticle aggregation, and poor adsorption of hydrophobic contaminants [24]. Researchers have investigated composite materials using TiO_2 in conjunction with carbon, WO_3, Bi_2O_3, ZnO, and SiO_2 to circumvent these restrictions [25-28].

Accordingly, to enhance the photocatalytic performance for water treatment applications, these adjustments are made to increase the surface area, raise catalyst recovery, promote charge separation, and improve visible light absorption [29]. The photocatalytic efficiency and stability of composites made with TiO_2 are greatly enhanced when SiO_2 is added. These composites are superior catalysts for the degradation of pollutants due to the synergistic effects brought about by the integration of SiO_2 with TiO_2. By increasing the effective surface area, SiO_2 enhances the photodegradation process on TiO_2 and contributes outstanding adsorption characteristics because of its network structure [30]. Composite materials made of SiO_2 and TiO_2 have a greater capacity to remove organic and inorganic contaminants when exposed to light, and due to the combined effects of silica's adsorption capacity and titania's photocatalytic ability [31]. Because of its low efficiency when exposed to sunlight and the expensive power requirements of artificial UV irradiation sources, photocatalytic wastewater treatment technology has few uses in the industrial sector of refineries. An important area of research is the optimization of photocatalytic efficiency through the development of novel photocatalysts, such as SiO_2/TiO_2 nanocomposites, which are suitable for the PRW treatment [32]. Concurrently, the design and optimization of photocatalytic wastewater treatment reactors (PWTRs) are crucial since insufficient reactor research and equipment sharing with other methods hinder industrial adoption [33].

Despite the considerable progress in TiO_2-based photocatalysis, most previous studies have focused on synthetic wastewater or single model pollutants under ideal laboratory conditions. Limited research has addressed the treatment of real petroleum refinery wastewater (PRW), which contains a complex mixture of recalcitrant organic compounds. Furthermore, insufficient attention has been given to the combined optimization of catalyst composition and reactor configuration under different irradiation sources.

In this context, this study introduces a new technology for treating real PRW from the Al-Diwaniya refinery plant in Iraq. It uses a SiO_2/TiO_2 nanocomposite catalyst, made by the sol–gel method at different molar ratios (20%, 10%, 5%, and 0% SiO_2 content labeled as S-20, S-10, S-5, and S-0 respectively) and different catalyst dosages (1, 2, and 3 g/L) under various light illumination (dark, visible, solar, UVC-8x8W, UVC-16x8W, and UVC-24x8W lights) within an AOPs system. To the best of our knowledge, this nanocomposite has not yet previously been applied for the treatment of real PRW under practical operating conditions. The study also features a newly designed photocatalysis reactor with a special geometric shape that improves photocatalytic efficiency. The main goal is to examine the performance of the system to reduce COD in PRW by exploring the influence of key variables, including the best catalyst loading ratio of S-5, catalyst dosage of 2 g/L, UVC lamps number of 8x8w, and reaction time of 4 h. This investigation aims to improve performance and offer a scalable model for use in industry.

2- Materials and methods

2.1. Characteristics of real refinery effluents

In this study, wastewater from the Al-Diwaniya oil refinery in Iraq served as a sample for research and investigation. The sample contained a mixture of heavy and light hydrocarbons and was collected prior to biological treatment and stored at 4ºC in the laboratory refrigerator until use. The refinery administration provides the characteristics of wastewater as listed in Table 1.

2.2. Chemicals

All chemicals used in this study were high-purity materials and were diluted with deionized water to the desired concentrations. The precursors of TiO_2 and SiO_2 were Titanium tetra isopropoxide (TTIP 97%) and tetra ethyl ortho silicate (TEOS 97%) respectively, they were obtained from Merck in Darmstadt, Germany. Ethanol C_2H_5OH (99.9%) was sourced from Rci Labscan in Bangkok, Thailand. Hydrochloric acid HCl and sodium hydroxide NaOH (both 99% pure) were purchased from Riedel-de Haen, Germany for pH adjustment. isopropanol C_3H_8O (99.8 %), sodium oxalate $Na_2C_2O_4$ (99.5 %), potassium dichromate $K_2Cr_2O_7$ (99 %), p-benzoquinone $C_6H_4O_2$ (99 %), and silver nitrate $AgNO_3$ (99 %) were all purchased from Sigma Aldrich-USA.

Table 1. Characteristics of Al-Diwaniya refinery wastewater

Parameter	Input	Output	Unit
pH	6.8	7.23	-
Temperature	25	22	ppm
TDS	5566	4898	ppm
Phenol	18.5	0.05	ppm
COD	500	102	ppm
BOD	180	20	ppm
Oil	25.2	11.6	ppm
Turbidity	33	7.29	NTU
PO_4^{3-}	0.12	0.8	ppm
Cl^-	900	450	ppm

2.3. Synthesis of photocatalysts

2.3.1. Synthesis of nanoparticles (TiO_2)

The detailed synthesis protocol for TiO_2 nanoparticles via the sol-gel method involves the following steps: titanium tetra isopropoxide (TTIP) is first mixed with pure ethanol, stirred for 30 minutes, followed by pH adjustment to 2 using dropwise addition of 2 M HCl, then distilled water addition and further mixing which leads to forming the gel. Once the gel dried for 24 h at 110°C, it was calcined for 2 h at 550°C to create TiO_2 nanoparticles. To modify the crystalline and structural characteristics of TiO_2 nanoparticles, this technique is like the one outlined by Vijayalakshmi and Rajendran [34]. The experimental steps of TiO_2 nanoparticles preparation are shown in Fig. 1.

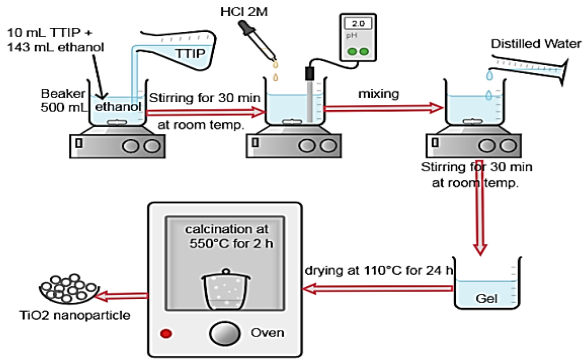

Fig. 1. The experimental steps of TiO_2 nanoparticles preparation

2.3.2. Synthesis of nanocomposite (SiO_2/TiO_2)

A binary oxide nanocomposite of SiO_2/TiO_2 with varying loading ratios of 20, 10, and 5 vol % was successfully prepared using the sol-gel technique. The synthesis utilized titanium tetra isopropoxide TTIP as the titania precursor and tetra ethyl ortho silicate TEOS as the silica precursor, with ethanol as a solvent. TTIP was added to ethanol in addressed amounts and combining them with TEOS, the mixture was agitated at room temperature for 30 minutes to begin the operation. The pH

of the solution was brought up to 3.5 by gradually adding 2 M HCl dropwise. After adding distilled water, the mixture was stirred for 30 more minutes until it turned into a gel. The final SiO_2/TiO_2 nanocomposite powder was made by drying the gel for 24 h at 110ºC and then calcining the powder for 2 h at 550ºC. This preparation method is aligned with previously reported studies [28, 35].

2.4. System design

Built on a semi-pilot scale and housed in a radiation chamber, a new photocatalytic reactor can be operated in the presence of both UV and visible light. To increase the efficiency and adaptability of photocatalytic processes, these reactors are engineered to accommodate photocatalysts that can use either visible or UV light. A variety of experimental and practical uses are possible because of the easy and flexible operation modes, which include batch and continuous operations. This apparatus is made up of two sections.

The first is a radiation chamber, which is a stainless-steel container in the shape of a hexagon with dimensions of 32 × 32 × 28 cm including 24 externally mounted UVC lamps, each measuring 254 nm, 8 W, 30 cm length, and 2.2 cm width to achieve a controlled light intensity of 64, 128, and 192 W/m² and maximize the photocatalytic degradation activity. In their study on wastewater treatment, Joseph et al. found that UVC lamp was more efficient than UVA lamp and UVB lamp in removing contaminants from wastewater Photocatalytic degradation of cationic dye simulated wastewater using four radiation sources, UVA, UVB, UVC and solar lamp of identical power output [36]. Based on their study, the type of lamps was selected. Zarei et al. confirmed these results, reinforcing UV-C's position as the most effective wavelength for photodegradation purposes [37]. The position of lamps was selected to be 10 cm from the reactor wall to ensure a reflective plane, improving the uniformity and dispersion efficiency of UV irradiation.

The second part represents by a larger hexagonal cover of wood (46 × 52 × 56 cm) encloses the stainless-steel container. Well controlled magnetic stirrer was used within the base to improve the reactants mixing efficiency ensuring uniform dispersion of the catalyst particles in the illuminated zone created by the UV lamps and reducing mass transfer limitations, thereby improving photocatalytic performance due to better exposure of catalyst surfaces to the reactants and light. To solve this problem of temperature rising inside the reactor hall caused by the UV light operation, two fans were positioned in front of the reactor to provide cool air, keep the temperature below 40ºC, and dissipate heat released by the UV lights, while a heat sensor connected to an automatic controller regulated the two fans operation to ensure temperature stability. For uniform heating distribution, the other two fans were turned on to circulate air within the chamber. The on/off timer capabilities were used to perform the automatic shutdown system as needed. To further optimize insulation and increase UV light utilization, the reactor was covered with aluminum foil and then covered with a layer of glass wool to reduce energy loss and keep the reactor environment under control both aided by aluminum foil's radiant barrier properties, which reflect up to 95% of radiant heat and UV radiation. The photocatalytic efficacy became much higher than in conventional batch or fixed-bed reactors because of reactor features like optimized light distribution, capability of continuous flow operation, and enhanced catalyst-contaminants interaction. Fig. 2 presents the setup of the photocatalysis process.

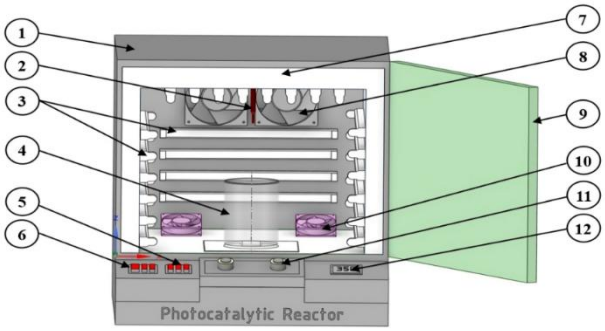

Fig. 2. The setup of the photocatalysis process includes wooden external cover (1), temperature sensor (2), UV lamps (3), reactor vessel (4), lamps controller (5), on/off button (6), stainless-steel container (7), cooling fan (8), the door (9), mixing fan (10), magnetic stirrer (11), and Temperature controller (12)

2.5. Characterization of the photocatalysts

The synthesized photocatalysts had their structural and compositional properties studied. The phases classification and content were identified using X-ray diffraction (XRD) utilizing Cu-Kα radiation (λ = 1.5406 Å) under a 2θ range of 20 - 80°, conducted using an Angstrom Advanced ADX2700 diffractometer. Functional groups on the catalyst surfaces were examined by Fourier transform infrared spectroscopy (FTIR) using a Bruker Vector 22 spectrometer in the range of 450–4000 cm^{-1} with the KBr pellet technique. The morphology of the samples was observed using a field-emission scanning electron microscope (FESEM, Inspect F50, FEI Company, Netherlands) and energy dispersive analysis by X-ray (EDAX) for quantitative analysis of the photocatalysts was conducted by the same device. Core AFM 2023 (Nanosurf AG, Switzerland) atomic force microscopy (AFM) was used to further evaluate the surface topography of both bare TiO_2 and SiO_2/TiO_2 ph. By utilizing ImageJ software on FESEM pictures, the average particle size of the two photocatalysts was ascertained.

To find the BET surface area and pore volume, the nitrogen adsorption-desorption isotherms were recorded using a method developed by Thermo Finnigan (USA). A 1 h pretreatment at 368 K and 3 h of post-treatment under nitrogen at 573 K were applied to the samples prior to measurement. The next step was to gather data at 77 K using a conventional 5-point BET nitrogen isotherm.

Analyses were conducted using a Micromeritics Gemini apparatus, which determines the volume of nitrogen absorbed and automatically calculates the surface area [38]. UV-Visible Diffuse Reflectance Spectroscopy (DRS) technique was used to estimate the optical characteristics of the synthesized photocatalysts were examined. The Avantes-Avaspec-2048 UV-Visible spectrophotometer was utilized to record the optical absorption analysis. The band gap energies of the produced photocatalysts' surfaces were calculated by measuring reflectance data R with a UV-visible spectrophotometer. It is outfitted with a Lab sphere integrating sphere diffuse reflectance accessory for DRS throughout the 300-500 nm range, using BaSO4 as a reference material. Photoluminescence (PL) Spectroscopy analysis of the synthesized photocatalysts was carried out with a Cary Eclipse Fluorescence Spectrometer, setting the excitation wavelengths to 330 nm for TiO2 and 380 nm for SiO2/TiO2 to capture their unique responses.

2.6. Photocatalysis procedure

The experiments were performed using UV irradiation at a temperature of 25 ± 2 °C. Before being treated in a batch-type photoreactor, 500 mL of real PRW (from the Al-Diwaniyah refinery in Iraq) was deposited into a 1 L reaction vessel. Utilizing a magnetic stirrer with 250 rpm, the wastewater was mixed with different photocatalyst amounts (1, 2, and 3 g/L) to conduct uniform dispersion. The catalyst particles and contaminated components were allowed to reach an adsorption-desorption equilibrium in the reactor vessel under dark conditions for 0.5 h prior to light illumination. Then, 8, 16, and 24 lamps (8 W each) of UV-C light were used to expose the composition along many reaction periods. To eliminate any leftover catalyst particles, samples were centrifuged and filtered through microfilter paper. The value of COD for PRW samples was measured using Lovibond instrument. Eq. 4 was used to calculate the percentage removal (RE%) of COD [39]:

$$RE\% = \frac{COD_i - COD_f}{COD_i} x100 \quad (4)$$

Where: COD_i and COD_f represent the initial and final contaminants concentration (mg/L) after time t of irradiation. An important and essential economic consideration in photocatalysis treatment processes is the consumption of Electrical Energy per Order (EE/O). Eq. 5 was used to compute EE/O for the photocatalytic treatment processes [40]:

$$EE/O = \frac{P*t}{V*\log(C_i/C_f)} x100 \quad (5)$$

where EE/O is the electrical energy per order (kWh/L), P is the power rating of the UV lamp (kW), t is the reaction time (h), V is the volume of the treated solution (L), C_i and C_f are the initial and final concentrations (COD) respectively.

2.7. COD measurements

Chemical Oxygen Demand (COD) is a measurement of the amount of oxidizing agent needed to react with a sample's contaminants in a controlled environment. In this study, the concentration of organic components in wastewater was indicated by COD. Based on the standard method (e.g., APHA 5220) [41], in a thermo-reactor (RD125, Lovibond) utilizing potassium dichromate ($K_2Cr_2O_7$) as the oxidizing agent, a 2 mL portion of wastewater was digested at 150 °C for 2 h to determine the COD value. A spectrophotometer (MD200, Lovibond) was used to measure the COD concentration of the digested sample once it had cooled to room temperature.

3- Results and discussions

3.1. Characterization of the photocatalysts

3.1.1. XRD analysis

The synthesized TiO_2 nanoparticles (symbolled as S-0), and S-20, S-10, and S-5, the mixed oxide materials prepared with different Si: Ti ratios (20:80, 10:90, and 5:95), show notable variations in diffraction peak intensities, revealing differences in material crystallinity, in their XRD patterns. Fig. 3a shows the XRD patterns of the bare TiO_2 and mixed oxide materials. All the peaks belong to the pure anatase phase TiO_2 (JCPDS 21-1272) [42], and there is a distinctive peak at $2\theta = 25.5°$ on these patterns. The strong crystallinity of the titania phase is shown by the high-intensity peaks observed in bare TiO_2 (S-0). Amorphous silica is responsible for the lack of SiO_2 peaks in all samples and the lower diffraction contrast in the TiO_2 anatase phase in SiO_2/TiO_2 mixed oxide materials.

However, at 2θ values of 25.5°, 38°, 48°, 55°, 63°, 69°, and 75° respectively, all the materials exhibit peaks that correspond to d101, d004, d200, d211, d204, d116, and d220. This confirms that the SiO_2/TiO_2 mixed oxide materials contain TiO_2 exclusively in the anatase phase [43]. The results show that the peak widens and crystallinity drops from 0% to 20% silica, due to an increase in the number of amorphous particles caused by the presence of additional SiO_2 particles in the SiO_2/TiO_2 composites, the crystallinity is decreased. Less sharp XRD peaks in the composite are evidence of this decrease. These observations correspond with prior research findings, as noted by Ho et al., 2020 [42].

3.1.2. FTIR analysis

The functional groups in bare TiO_2 and SiO_2/TiO_2 composites were identified using FTIR as a later analytical approach in the 450-4000 cm^{-1} wave number range. Fig. 3b shows the FTIR of titania nanoparticles with different amounts of silica and without silica. The stretching vibration of -OH is reflected in the spectra at 3402-3435 cm^{-1}, while the bending vibration of -OH is represented by the band at 1630 cm^{-1} [44]. The water band in samples of pure calcined titania and synthesized Si/Ti showed a rise as the TiO_2 content rose, due to the O-H stretching of defective Si-OH groups and residual water. The two small bands observed at 2850 and 2920

cm^{-1} were caused by organic species that remained after rinsing the TiO_2 powders with distilled water.
These compounds were employed as precursors throughout the synthesis [45]. One signal observed at 1050-1130 cm^{-1} is thought to be caused by the asymmetric stretching vibration of Si-O-Si bonds [46]. According to the findings from XRD and FTIR, silica is present in an amorphous phase [47]. Ti-O-Ti bond stretching vibration corresponds to the peaks found at 657-696 cm^{-1} [48]. Because of the high surface water adsorption, these peaks become more prominent as the SiO_2 content increases [49]. It appears that SiO_2 has an active O-H side for surface reactions, based on the difference in O-H intensity between the two compounds [13].

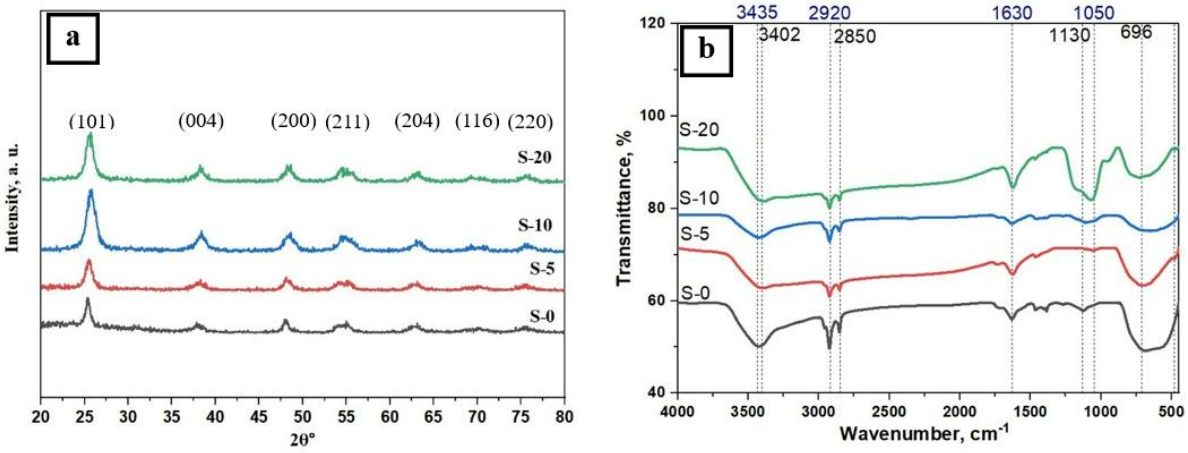

Fig. 3. The XRD pattern (a) and the FTIR spectra (b) for prepared bare TiO_2 and SiO_2/TiO_2 composites

3.1.3. FESEM and EDAX analysis

The morphological properties of the prepared nanoparticles were investigated using FESEM. The morphology of SiO_2/TiO_2 nanocomposites with different SiO_2/TiO_2 weight percentages (S-20, S-10, and S-5), as well as bare TiO_2 (S-0), is shown in the FESEM pictures shown in Fig. 4. These findings provide credence to the idea that particles have a spherical shape. Furthermore, the FESEM micrographs show that the nanocomposite is made up of mesoporous aggregates, and the aggregation level increases with increasing silica content because amorphous silica accumulates on the TiO_2 surface (as illustrated in Fig. 4a and Fig. 4b). These results are in agreement with what was found by XRD analysis. In their 2013 study, Siddiqa et al. [50] found similar results while studying SiO_2/TiO_2 nanocomposites. The need to create composite materials is confirmed by Fig. 4d, which shows that TiO_2 particles have a tendency to agglomerate. S-20, S-10, S-5, and S-0 fell into the following particle sizes: 198.16, 59.82, 56.25, and 96.66 nm, in that order. This result emphasizes the optimum performance of 5% SiO_2/TiO_2 (S-5) through producing particles with smallest size as shown in Fig. 4c. Using FESEM images, the Image J software validated these findings.

EDAX analysis was used to specify the elemental composition of the synthesized catalysts. The results are illustrated in Fig. 5. This study supports the findings of other scientists conducting study in this field [42, 51, 52].

3.1.4. AFM analysis

Fig. 6 shows the 3D images of the surface features of the synthesized SiO_2/TiO_2 photocatalysts with different weight ratios (S-20, S-10, and S-5), as well as bare TiO_2 (S-0), generated by the AFM analysis. There were more depressions than elevations in the images, indicating that the particles were evenly distributed. Images captured by AFM are more accurate in depicting the surface features and particle size distribution of the samples than those captured by FESEM. The average particle sizes, skewness values, root mean square (Sq), average roughness (Sa), and kurtosis parameter are all listed in Table 2. Data that was left-skewed, meaning the left tail was longer than the right, was represented by negative skewness values. Flat tops and steep dips were features of the surfaces. The surface profile had strong peaks and deep troughs, as assessed by the kurtosis parameter; these findings were in agreement with Khataee et al., [51].

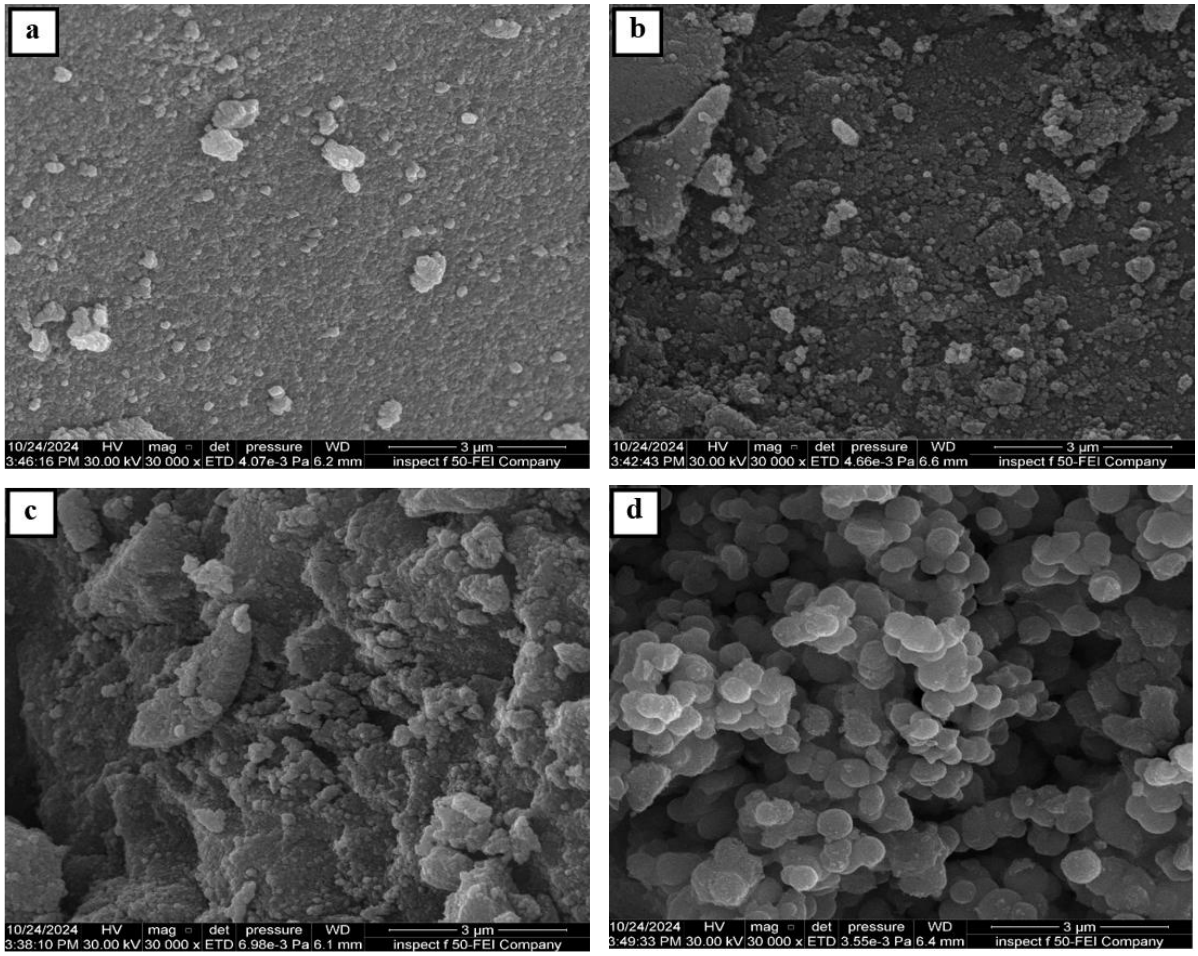

Fig. 4. FESEM images for (a) 20% SiO_2/TiO_2, (b) 10% SiO_2/TiO_2, (c) 5% SiO_2/TiO_2, and (d) bare TiO_2

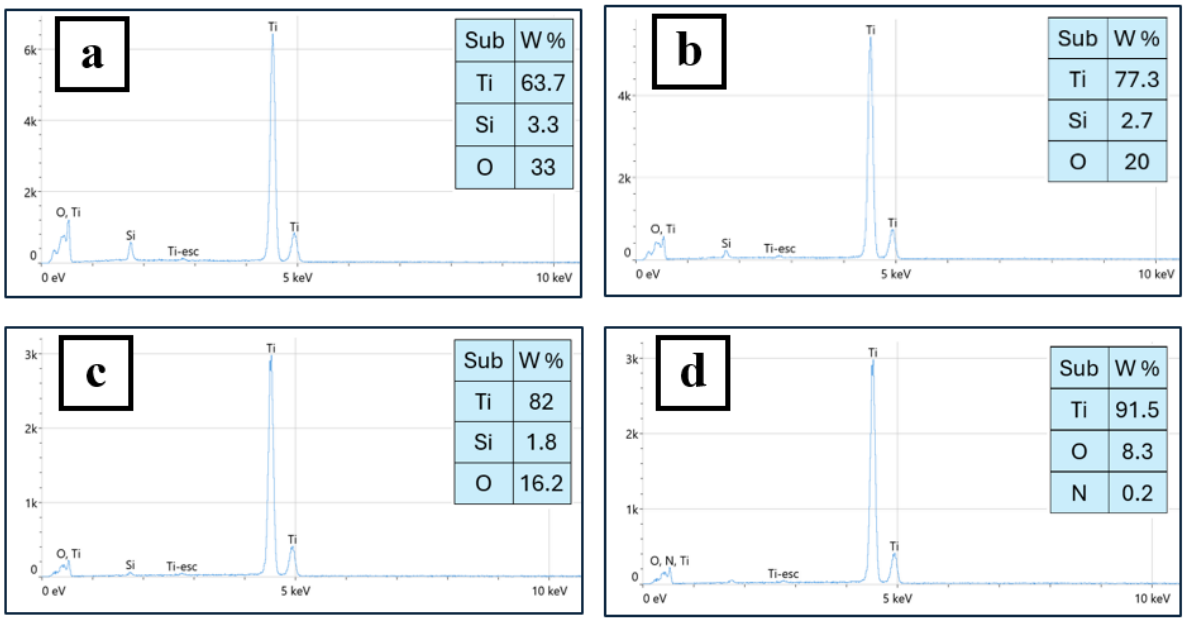

Fig. 5. FDAX results for (a) 20% SiO_2/TiO_2, (b) 10% SiO_2/TiO_2, (c) 5% SiO_2/TiO_2, and (d) bare TiO_2

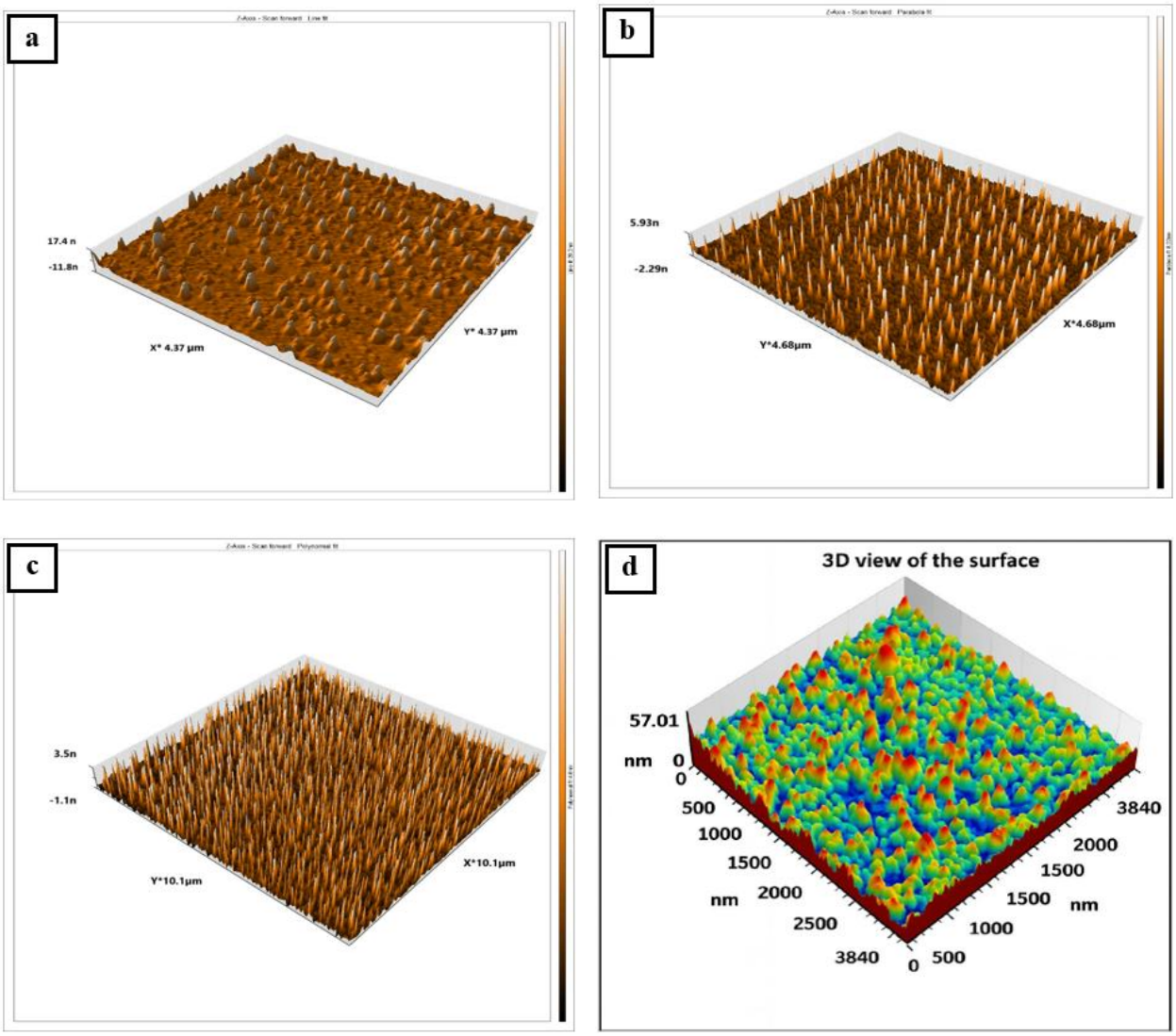

Fig. 6. AFM images for (a) 20% SiO_2/TiO_2, (b) 10% SiO_2/TiO_2, (c) 5% SiO_2/TiO_2, and (d) bare TiO_2

Table 2. Results of AFM parameters

Sub.	root mean square (Sq)	average roughness (Sa)	kurtosis parameter	skewness	average particle diameters, nm
S-20	103.45	84.68	2.158	-0.387	218.2
S-10	37.42	16.72	67.93	7.484	65.25
S-5	7.742	5.839	3.706	0.666	61.94
S-0	6.598	5.582	3.518	0.729	93.58

3.1.5. BET analysis

Table 3 summarizes the textural properties, such as BET surface area and pore volume, of the prepared bare TiO_2 (S-0) and photocatalyst nanocomposites with varied SiO_2/TiO_2 ratios (S-20, S-10, and S-5). According to the results, the surface area grows in direct correlation with the concentration of SiO_2 in the nanocomposites. The surface area of fabricated SiO_2/TiO_2 samples is much higher than that of bare TiO_2. The optimum ratio, S-5, shows a bigger pore volume than the other samples. This is because the amorphous SiO_2 has a larger surface area, as shown by XRD measurements. To keep the produced catalyst's mesoporosity intact and avoid the collapse of hole channels, which would otherwise reduce the number of active sites available for photocatalysis activities, SiO_2 inclusion is critical [52]. More active sites for photocatalytic processes are associated with a bigger BET surface area, which could lead to better degradation efficiency. This occurs because the photocatalyst has more opportunities to interact with pollutants when its surface area is greater and its enhanced light absorption capabilities further improve the removal efficiency of the process. Although the BET surface area increased with higher SiO_2 content, the photocatalytic activity did not follow the same trend. This behavior can be attributed to the non-photoactive nature of SiO_2, which at higher loadings partially shields TiO_2 active sites, reduces photon absorption efficiency, and limits charge carrier generation. Consequently, excessive SiO_2 content may

enhance adsorption but does not necessarily improve reactive species formation, leading to reduced overall degradation performance [43, 53].

Table 3. The nitrogen adsorption/desorption isotherm results

Catalyst	BET surface area (m^2/g)	Pore volume (m^3/g)
Bare TiO_2 (S-0)	54.67	0.11
5% SiO_2/TiO_2 (S-5)	168.95	0.21
10% SiO_2/TiO_2 (S-10)	171.61	0.18
20% SiO_2/TiO_2 (S-20)	180.72	0.13

3.1.6. UV-DRS Analysis

An essential consideration in photocatalysis research investigations is the measurement of the energy band gap (E_{bg}). The optical E_{bg} was estimated using the Kubelka–Munk function assuming an indirect allowed transition as shown in Fig. 7. The results were achieved by extrapolating the linear region of the spectra $(F(R)hv)^{1/2}$ vs. hv). The E_{bg} of bare TiO_2 was found to be 3.1 eV, while that of S-5 was 2.9 eV. The variation in the E_{bg} values can be elucidated by the alterations in the E_{bg} of the TiO_2 due to the presence of SiO_2 leading to the formation of Ti–O–Si bonds, which modifies the electronic structure [1]

DRS analysis confirms that the S-5 composite is not merely a physical mixture but an electronically integrated material. The engineered reduction in its band gap is a direct consequence of the formed Ti–O–Si interface, making it a more responsive photocatalyst within the designed reactor's irradiation field. This property, combined with its superior textural and charge transport characteristics, promotes its exceptional performance in mineralizing organic contaminants from real, complex PRW. Similar observations were stated by [13].

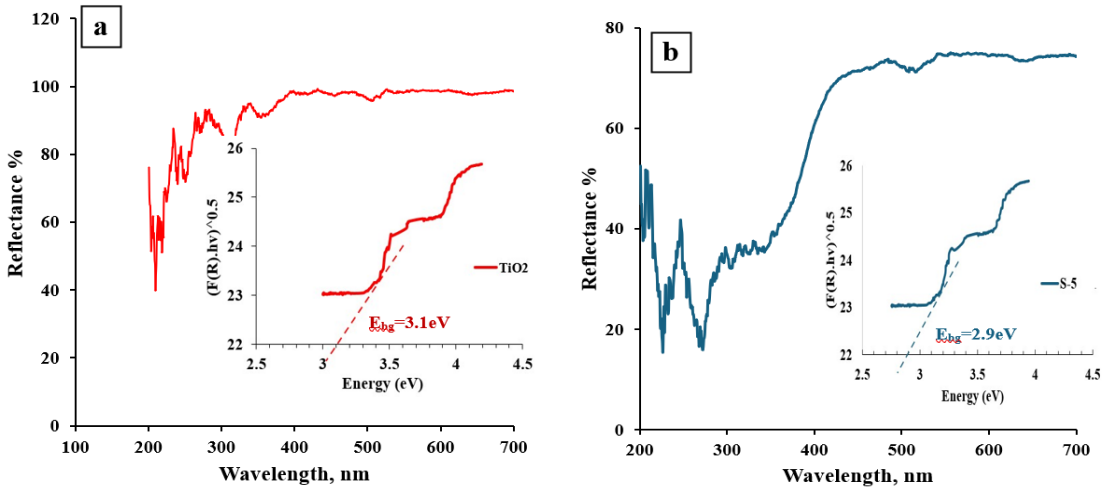

Fig. 7. UV-DRS spectra and T_{auc} plots for band gap estimation of (a)Bare TiO_2 and (b)S-5 nanocomposite

3.1.7. PL Analysis

PL analysis is employed to evaluate the efficiency of charge carriers and to investigate the recombination behavior of photogenerated electron–hole pairs in semiconductor materials. A high PL emission intensity indicates poor charge separation accompanied by rapid electron–hole recombination, whereas a low PL emission intensity reflects suppressed recombination and more efficient charge transfer of electrons. As illustrated in Fig. 8, bare TiO_2 exhibits a moderate performance characterized by a relatively high PL intensity of approximately 395 a.u., suggesting pronounced electron–hole recombination. In contrast, S-5 composite performs better as shown by its significantly lower PL intensity of roughly 260 a.u., which indicates improved charge separation and decreased recombination.

Notably, there is no significant shift in emission peak position observed, indicating that the modification mainly affected recombination dynamics rather than introducing new deep-level defects.

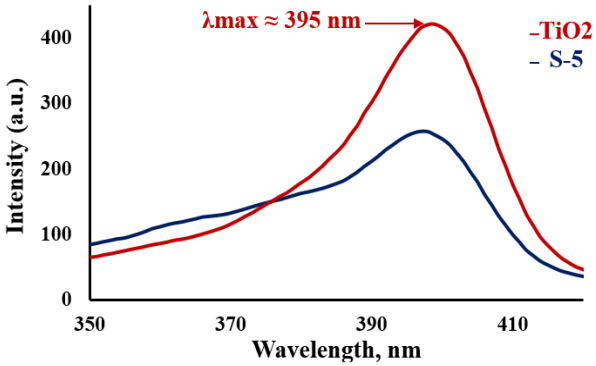

Fig. 8. PL Spectra of bare TiO_2 and S-5 nanocomposite

3.2. Photocatalytic degradation of COD

3.2.1. Effect of SiO_2/TiO_2 loading ratio

The molar ratio of the prepared SiO_2/TiO_2 nano photocatalyst has a notable effect on COD reduction under UV light at a wavelength of 254 nm. As shown in

Fig. 9, the S-5 sample showed the best photocatalytic performance, reaching 90% degradation under optimal conditions: 2 g/L catalyst dosage, 4 h of irradiation, and 8 x 8 W intensity. While the S-20 shows the poorest removal efficiency, even less than bare TiO_2. Subsequently, Silica content plays a main role in the enhancement of performance by multiplying amorphous particles within the composites, which in turn supercharges their photocatalytic power. Acting as a natural adsorbent, the SiO_2 substrate expands the composite's surface area, allowing it to tackle and break down even more pollutants [54]. Moreover, when the silica content was higher than 5%, the photocatalytic activity went down because SiO_2 itself does not have high photocatalytic properties. The remarkable performance of S-5 can be attributed to its consistently ultra-fine particles. This increases its surface area and improves its ability to reduce COD, as demonstrated in Table 3. These results are in agreement with what Sikong et al. found in 2008 [35]. Finally, out of all the samples examined, the S-5 photocatalyst distinguishes with its outstanding capacity to eliminate organic pollutants, proving that its loading ratio is the most effective.

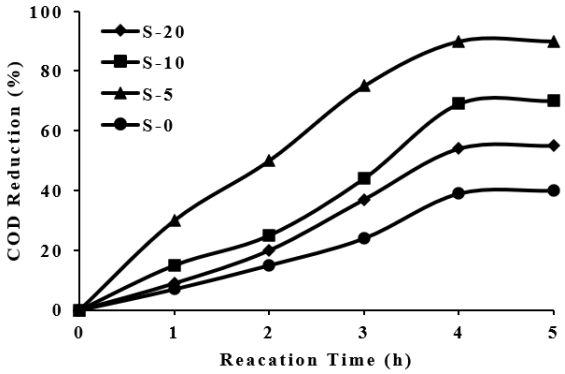

Fig. 9. Effect of the molar ratio of SiO_2/TiO_2 on the COD reduction

3.2.2. Effect of SiO_2/TiO_2 dosage

The performance and cost of photocatalyst can be optimized by finding the optimal catalyst dosage. Insufficient amount of catalysts requires longer light exposure and extended retention times, thereby increasing operational cost. Conversely, excessive amount of catalysts not only raise costs but also hinder photoactivity by making the suspension turbid [38]. In this investigation, the researchers set out to examine how changing the amount of photocatalyst would affect COD removal with a range of catalyst dosages, from 1 to 3 g/L, exposing to UV light for 4 h. As illustrated in Fig. 10, COD reduction was improved by increasing the photocatalyst dosage until reaching a point of equilibrium, surpassing this point led to decrease the removal efficiency. The optimal degradation was found at 2 g/L, where COD oxidation peaked at 90% after 4 h at equilibrium.

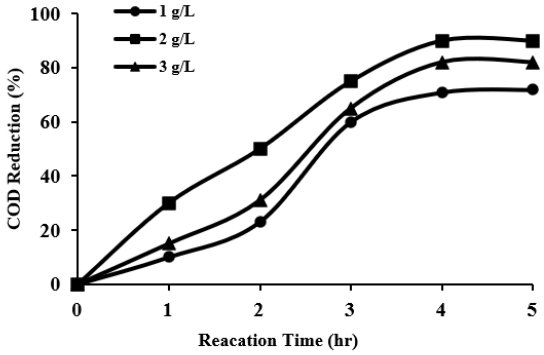

Fig. 10. Effect of SiO_2/TiO_2 dosage on COD reduction

3.2.3. Effect of light type

The type and intensity of the applied lamps influence the performance of the photodegradation of organic pollutants [55]. The reduction of COD in real PRW was investigated at various light sources including the dark, visible light, sun light, and UV light as illustrated in Fig. 11. The work was carried out under specific conditions comprising a SiO_2/TiO_2 dosage of 2 g/L, SiO_2/TiO_2 loading ratio of 5/95% (S-5) , and reaction time of 4 h. exposed to identical conditions without a catalyst, yielding a minimal COD degradation of approximately 1.5% after 4 h. Fig. 9 shows the results of COD reduction using SiO_2/TiO_2 photocatalyst was 7% in the dark, 18% in visible light and 40% in the sun light after 4h. whereas, utilizing UVC light achieved maximum COD degradation efficiency of 90% after 4 h. these outcomes revealed the effective performance of the degradation under UV irradiation. The complexity of the real PRW, on the other hand, makes the degradation's poor performance obvious in dark and other types of illumination. The high removal efficiency under UV illumination can be attributed to improving the photodegradation process by increasing the generation of the free radicals responsible for contaminants degradation in wastewater including hydroxyl radical ($^{\bullet}OH$) and superoxide ($^{\bullet}O_2^-$) after absorption the photon energy released from UV irradiation.

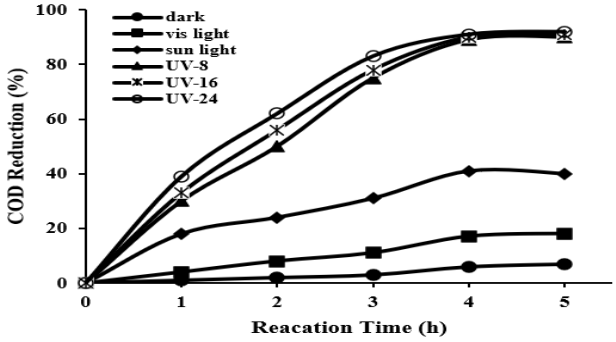

Fig. 11. Effect of light type on the COD reduction

Although UV-24 (192W) achieves a marginally higher COD reduction of 91%, its advantage over UV-8 (64W) and UV-16 (128W) is barely noticeable. Based on both capital and energy costs, UV-8 emerges as the most cost-effective option. This result is supported by the consumption power data for each case, calculated using Eq. 5 and presented in Table 4.

Table 4. The consumption power (EE/O) for different intensities

No.	No. of lamps (UV-C)	Time (h)	EE/O (kWh/L)
1	8 x 8W	4	0.512
2	16 x 8W	4	1.024
3	24 x 8W	4	1.536

3.3. Kinetic study

For photocatalytic process models involving COD reduction, first-order analysis is commonly used, particularly in cases when the substrate concentration is present in small amounts. As shown in Eq. 6: the reaction rate (r) at which COD vanishes is directly related to its concentration, leading to the famous pseudo-first-order kinetic model [56]:

$$r = -\frac{dC}{dt} = kC \quad (6)$$

Where: k is the first order rate constant. Eq. 7 can be obtained after integrating Eq. 6 as follows:

$$\ln\left(\frac{C}{C_0}\right) = -kt \quad (7)$$

Where Co denotes the initial concentration of COD (ppm), C is the concentration of COD (ppm) at any time t. The slope obtained from plotting -ln (Co/C) versus t provides the rate constant k. Fig. 12 shows a strong linear relationship between ln (Co/C) and reduction time for the photocatalysts that were evaluated. This clearly shows that the process follows pseudo–first-order model, as the Langmuir-Hinshelwood model says it should.

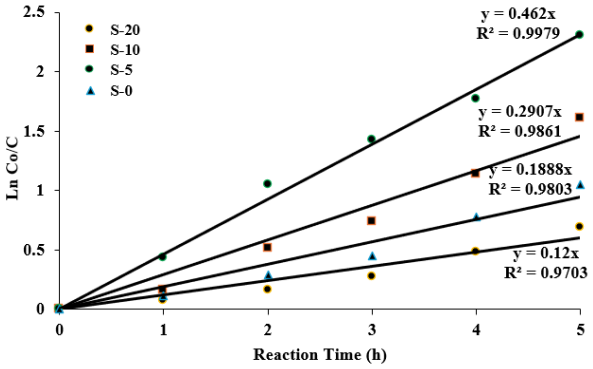

Fig. 12. Photocatalytic kinetic model for SiO_2/TiO_2 and TiO_2 nanoparticles, under UV irradiation

Table 5 illustrates that the high correlation coefficients (R^2) reflect how well the practical data fits the linear fit, which confirms that this kinetic model is reliable. The estimated rate constants (k) demonstrate that the S-5 photocatalyst has a faster reaction rate (k = 0.463 h^{-1}) comparing with the other photocatalysts. The significant increase in the reaction rate for S-5 can be attributed to its extensive surface area with greater pore volume (as shown in Table 3), enhanced active sites distribution, and lower electron–hole recombination.

Table 5. The kinetic properties of the photocatalysts

Photocatalysts	Kinetics Equation	k_1 (min^{-1})	R^2
Bare TiO_2 (S-0)	ln (Co/C) = 0.189 t	0.189	0.980
5% SiO_2/TiO_2 (S-5)	ln (Co/C) = 0.463 t	0.463	0.998
10% SiO_2/TiO_2 (S-10)	ln (Co/C) = 0.290 t	0.290	0.986
20% SiO_2/TiO_2 (S-20)	ln (Co/C) = 0.120 t	0.120	0.970

3.4. Catalyst reusability

Under controlled conditions, the photocatalyst was reused five cycles of COD photodegradation to examine its reusability after multi-washing, drying and sintering. With a catalyst dose of 2 g/L, a reaction time of 4 h, and UV-C light source. Fig. 13 shows that the S-5 showed remarkable endurance and even after five cycles, its performance dropped little from 90% to 82.4%, revealing its excellent level. The photocatalyst's capacity to efficiently eliminate organic particles from polluted water is demonstrated by this outcome. The minor decrease in activity likely resulted from photocatalyst loss during washing [57], while the organic contaminated particles buildup may have blocked pores and reduced active sites [58]. Transforming waste solids into a highly efficient, reusable SiO_2/TiO_2 photocatalyst offers a promising new approach for removing all kinds of pollutants from wastewater.

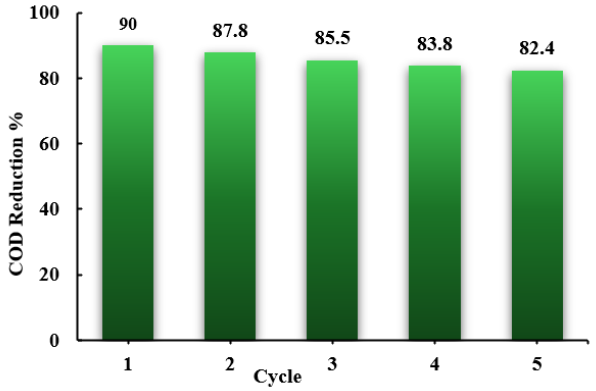

Fig. 13. The reusability study of SiO_2/TiO_2 (S-5)

3.5. Scavenger experiments

The reduction of COD happens through the action of several reactive species, including electrons (e^-), holes (h^+), hydroxyl radicals ($^{\bullet}OH$), and superoxide radicals ($^{\bullet}O_2^-$). The photocatalytic degradation mechanism follows typical AOPs pathways involving the generation of hydroxyl radicals (•OH) and superoxide radicals ($\bullet O_2^-$), which are primarily responsible for COD reduction in refinery wastewater systems. To specify which of these

play the main role, we introduced specific scavengers $AgNO_3$, $Na_2C_2O_4$, C_3H_8O and $C_6H_4O_2$ each used to trap a particular species [59], as illustrated in Fig. 14. Using real PRW, we set the stage with a photocatalyst dosage of 2 g/L, SiO_2/TiO_2 ratio of 5/95% (S-5), a 1000 mL treated volume, letting the reaction run for 4 h under UV-C light. The results were telling $AgNO_3$ exhibited the less performance, while $Na_2C_2O_4$ reached COD degradation of 50%. The most dramatic drops came with C_3H_8O and $C_6H_4O_2$, revealing that superoxide and hydroxyl radicals are the main drivers of COD photodegradation. The hierarchy sequence among these reactive species is illustrated by the order of effectiveness: superoxide, hydroxyl radicals, holes, and electrons. This suggests that electron transfer from the conduction band of TiO_2 to dissolved oxygen is a key step in generating reactive oxygen species. The results confirm that the photocatalytic degradation mechanism is primarily governed by oxidative radical pathways, which are consistent with the intrinsic charge separation behavior of TiO_2-based systems under irradiation.

Although optical analyses (DRS and PL) provide insight into band structure and charge carrier recombination, enhanced photocatalytic activity arises from the synergistic interplay between electronic and structural modifications. DRS confirmed effective UV-C activation, PL indicated suppressed electron–hole recombination, and BET analysis revealed increased surface area and pore volume that promoted reactive oxygen species generation, as verified by scavenger experiments.

The novelty of this work lies in directly linking charge-separation efficiency with surface structural enhancement and radical-mediated degradation within one coherent photocatalytic system.

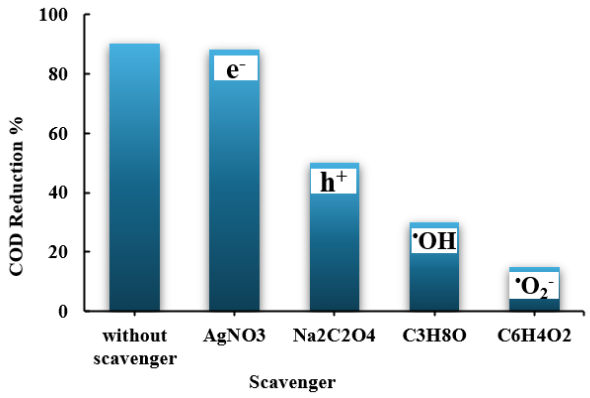

Fig. 14. The scavenging study of SiO_2/TiO_2 (S-5)

3.6. Comparison with previous work

Prior studies employed SiO_2/TiO_2 on simulated water containing phenols or dyes in AOPs; however, this study is the first to conduct UV/SiO_2/TiO_2 to genuine PRW. The efficiency of COD reducing, the photocatalyst surface area, and the process parameters were compared with previous studies in Table 6. Compared to previous photocatalysts used for PRW, our technology proved to be quite successful in treating real wastewater containing complex organic molecules. As illustrated in Table 1, the approach necessitated a longer time is related to the varied contaminants present in real PRW, despite our better COD removal efficiency (90%). It is crucial for real-world applications to strike a balance between efficiency and reaction time. Table 6 shows that the photocatalytic technique is affected by the photocatalyst surface area, and that this effect varies for various organic pollutants. In general, our findings outperform earlier studies according to surface area and removal effectiveness.

Table 6. Comparison of the current study with previous studies for PRW treatment by photocatalytic technique

Experimental conditions	Light source	Surface area m^2/g	RE%	Ref.
TiO_2 dosage of 2 g/L, airflow rate of 1.04 L/min, and time of 30 min	UV-C	50	66 phenols 81 **SOG	[60]
SnO_2 dosage of 0.1 g/L, pH of 3, and time of 99 min	UV-C	29	73.16 COD	[61]
TiO_2 (*Degussa P25) dosage of 8 g/L, aeration flow of 1.225 L/min, and time of 90 min	UV-C	50	76 phenol 88 oil	[62]
TiO_2 (*P25) dosage of 0.1 g/L, pH = 3, and time = 2 h	UV-C	***ND	78	[63]
The photocatalyst SiO_2/TiO_2 dosage = 2 g/L, intensity 8 x 8W, and time = 4 h	UV-C	168.95	90 COD	Present work

*Degussa P25 means (80% anatase, 20% rutile), **SOG is Power Glide SAE40 motor vehicle oil, and *** ND refers to Not Detected

4- Conclusion

This study demonstrated the effectiveness of sol–gel synthesized bare TiO_2 and the SiO_2/TiO_2 nanocomposites fort treating real and complicated PRW from the Al-Diwaniya refinery. By focusing on COD removal, the work found that the best SiO_2/TiO_2 ratio was 5:95 (S-5) due to its much smaller particle size, improved surface area, and enhanced active site distribution. The main reason behind this improvement was a newly designed photocatalytic reactor, built locally, and it had advanced features that helped in breaking down and mineralizing COD under UV- C light. The experiments showed that S-5 nanocomposite reduced COD by approximately 90 % with the optimal conditions of 5/95% SiO_2/TiO_2 loading ratio, 2 g/L dosage, and 4 h reaction time under 8 lamps of UV-C illumination (8W each lamp), whereas the bare TiO_2 only reduced COD by about 40% under the same conditions, with total consumption energy used of just 0.512 kWh/L.

The results of the kinetic study confirmed that the reaction behavior fitted with the pseudo first order model with high correlation coefficients (R^2) of 0.998 and rate constant of 0.463. The reusability examination revealed that the photocatalyst kept most of its activity through five repeated cycles, which proves its stability and can be utilized widely for wastewater treatment. Scavenger tests exhibited that, the dominant reactive species responsible

for the reduction of COD from PRW was the $^{\bullet}O_2^-$ radical in the first class, followed by $^{\bullet}OH$, h^+, and e^-.

Overall, the strong combination of the optimized SiO_2/TiO_2 catalyst loading ratio and the new innovative reactor design gave excellent COD removal efficiency and represents a feasible, cost-effective, and environmentally friendly solution for real wastewater treatment in the ongoing efforts to safeguard the environment.

Acknowledgement

The authors express their gratitude for the invaluable insights, assistance, and technical assistance they received from the staff of the Department of Chemical Engineering, College of Engineering, University of Baghdad.

References

[1] S. Adday and S. M. Al-Jubouri, "Developing a versatile visible-light-driven polyvinylidene fluoride/Ag_2O@CRA photocatalytic membrane for efficient treatment of organic pollutants-contained wastewater," *Journal of Water Process Engineering*, vol. 73, 2025, https://doi.org/10.1016/j.jwpe.2025.107713

[2] Q. K. Hameed and W. T. Mohammed, "Treatment of Wastewater from Oil Refineries by a Combination of Electrocoagulation with Photocatalytic Processes Using Immobilized Nano-Zinc Oxide Photocatalyst," *Journal of Ecological Engineering*, vol. 25, no. 11, pp. 109–123, 2024, https://doi.org/10.12911/22998993/192671

[3] H. Diya'Uddeen, W. M. A. W. Daud, and A. R. Abdul Aziz, "Treatment technologies for petroleum refinery effluents: A review," *Process Safety and Environmental Protection*, vol. 89, no. 2, pp. 95-105, 2011, https://doi.org/10.1016/j.psep.2010.11.003

[4] M. M. Jiad and A. H. Abbar, "Treatment of Petroleum Refinery Wastewater by Sono Fenton Process Utilizing the in-Situ Generated Hydrogen Peroxide," *Al-Khwarizmi Engineering Journal*, vol. 19, no. 2, 2023, https://doi.org/10.22153/kej.2023.04.002

[5] K. Kanaujiya, T. Paul, A. Sinharoy, and K. Pakshirajan, "Biological Treatment Processes for the Removal of Organic Micropollutants from Wastewater: A review," *Current Pollution Reports*, vol. 5, pp. 112-128, 2019, https://doi.org/10.1007/s40726-019-00110-x

[6] A. G. Saleem and S. M. Al-Jubouri, "Efficient separation of organic dyes using polyvinylidene fluoride/polyethylene glycol-tin oxide (PVDF/PEG-SnO_2) nanoparticles ultrafiltration membrane," *Applied Science and Engineering Progress*, vol. 17, no. 4, p. 7523, 2024, https://doi.org/10.14416/j.asep.2024.08.001

[7] Z. A. Ibrahim and A. F. Al-Alawy, "Synthesis and characterization of dual functional potassium doped MWCNT composites (K@Fe_3O_4@MWCNT and TEG-K/MWCNT) as innovative osmotic agents for forward osmosis processes," *Journal of Molecular Liquids*, vol. 437, 2025, https://doi.org/10.1016/j.molliq.2025.128452

[8] S. M. Al-Jubouri, H. A. Al-Jendeel, S. A. Rashid, and S. Al-Batty, "Antibiotics adsorption from contaminated water by composites of ZSM-5 zeolite nanocrystals coated carbon," *Journal of Water Process Engineering*, vol. 47, no. January, p. 102745, 2022, https://doi.org/10.1016/j.jwpe.2022.102745

[9] Dr. T. J. M. Mohammed, S. I. H. Habeeb, Z. K. K. Kreamid, and A. A. A. Ali, "Treatment of Refinery Industry Wastewater Using Ion Exchange Technology and Studies Kinetics and Thermo-dynamic Parameters," *Journal of Petroleum Research and Studies*, vol. 8, no. 3, 2018, https://doi.org/10.52716/jprs.v8i3.254

[10] S. M. Al-Jubouri *et al.*, "Multicomponent Equilibrium Isotherms and Kinetics Study of Heavy Metals Removal from Aqueous Solutions Using Electrocoagulation Combined with Mordenite Zeolite and Ultrasonication," *Applied Science and Engineering Progress*, vol. 18, no. 1, p. 7484, 2025, https://doi.org/10.14416/j.asep.2024.07.011

[11] K. M. Abed, B. M. Kurji, S. A. Rashid, and B. A. Abdulmajeed, "Kinetics and Thermodynamics of Peppermint Oil Extraction From Peppermint Leaves," *Iraqi Journal of Chemical and Petroleum Engineering*, vol. 20, no. 4, pp. 1–6, 2019, https://doi.org/10.31699/ijcpe.2019.4.1

[12] A. Khalidi-Idrissi, O. Hartal, A. Madinzi, K. El-Abbadi, and S. Souabi, "Natural flotation and coagulation–flocculation: a dual approach to refinery wastewater treatment," *Euro-Mediterranean Journal for Environmental Integration*, vol. 10, no. 3, 2025, https://doi.org/10.1007/s41207-024-00558-4

[13] R. Eddy *et al.*, "Photocatalytic phenol degradation by silica-modified titanium dioxide," *Applied Sciences (Switzerland)*, vol. 11, no. 19, 2021, https://doi.org/10.3390/app11199033

[14] J. O. Tijani, O. O. Fatoba, G. Madzivire, and L. F. Petrik, "A review of combined advanced oxidation technologies for the removal of organic pollutants from water," *Water, Air, & Soil Pollution*, vol. 225, no. 9, 2014, https://doi.org/10.1007/s11270-014-2102-y

[15] S. O. Tebbi *et al.*, "Green Synthesis of Sustainable and Cost-Effective TiO_2-SiO_2-Fe_2O_3 Heterojunction Nanocomposites for Rhodamine B Dye Degradation Under Sunlight," *Water (Switzerland)*, vol. 17, no. 2, 2025, https://doi.org/10.3390/w17020168

[16] W. F. Elmobarak, B. H. Hameed, F. Almomani, and A. Z. Abdullah, "A Review on the Treatment of Petroleum Refinery Wastewater Using Advanced Oxidation Processes," *Catalysts*, vol. 11, no. 7, 2021, https://doi.org/10.3390/catal11070782

[17] S. M. Lam, J. A. Quek, and J. C. Sin, "Mechanistic investigation of visible light responsive Ag/ZnO micro/nanoflowers for enhanced photocatalytic performance and antibacterial activity," *Journal of Photochemistry and Photobiolgy A: Chemistry*, vol. 353, pp. 171-184, 2018, https://doi.org/10.1016/j.jphotochem.2017.11.021

[18] A. Chakravorty and S. Roy, "A review of photocatalysis, basic principles, processes, and materials," *Sustainable Chemistry for the Environment*, vol. 8, 2024, https://doi.org/10.1016/j.scenv.2024.100155

[19] K. T. Amakiri, A. Angelis-Dimakis, and A. R. Canon, "Recent advances, influencing factors, and future research prospects using photocatalytic process for produced water treatment," *Water Science and Technology*, vol. 85, no. 3, 2022, https://doi.org/10.2166/wst.2021.641

[20] Friedmann, "A General Overview of Heterogeneous Photocatalysis as a Remediation Technology for Wastewaters Containing Pharmaceutical Compounds," *Water*, vol. 14 no. 21, 2022. https://doi.org/10.3390/w14213588

[21] D. Rosa, G. Cimini, M. P. Bracciale, A. C. Felici, and L. Di Palma, "Iron-doped titania nanoparticles supported on polystyrene for photocatalytic treatment of contaminated water in a continuous system," *Journal of Photochemistry and Photobiolgy A: Chemistry*, vol. 447, 2024, https://doi.org/10.1016/j.jphotochem.2023.115241

[22] K. Rajeshwar, C. R. Chenthamarakshan, S. Goeringer, and M. Djukic, "Titania-based heterogeneous photocatalysis. Materials, mechanistic issues, and implications for environmental remediation," in *Pure and Applied Chemistry*, 2001. https://doi.org/10.1351/pac200173121849

[23] N. S. Topare, M. Joy, R. R. Joshi, P. B. Jadhav, and L. K. Kshirsagar, "Treatment of petroleum industry wastewater using TiO_2/UV photocatalytic process," *Journal of the Indian Chemical Society*, vol. 92, no. 2, pp. 219–222, 2015.

[24] S. M. Park *et al.*, "Hybrid CuxO-TiO_2 Heterostructured Composites for Photocatalytic CO_2 Reduction into Methane Using Solar Irradiation: Sunlight into Fuel," *American Chemical Society Omega*, vol. 1, no. 5, 2016, https://doi.org/10.1021/acsomega.6b00164

[25] L. Belhomme *et al.*, "Investigation of the Photochromism of WO_3, TiO_2, and Composite WO_3-TiO_2 Nanoparticles," *Inorganic Chemistry*, vol. 63, no. 21, 2024, https://doi.org/10.1021/acs.inorgchem.4c01379

[26] V. Ruiz-Santoyo, S. García-Carvajal, and M. C. Arenas-Arrocena, "Photocatalytic removal of synthetic dyes using Bi_2O_3–TiO_2 nanocomposites obtained by simple hydrothermal route," *Journal of Nanoparticle Research*, vol. 27, no. 2, 2025, https://doi.org/10.1007/s11051-024-06207-9

[27] D. A. D. A. Aljuboury, P. Palaniandy, H. B. A. Aziz, S. Feroz, and S. S. A. Amr, "Evaluating photo-degradation of COD and TOC in petroleum refinery wastewater by using TiO_2/ZnO photo-catalyst," *Water Science and Technology*, vol. 74, no. 6, 2016, https://doi.org/10.2166/wst.2016.293

[28] N. F. Azlan, S. Akhbar, S. H. Hanipah, and R. W. Sharudin, "A short review on synthesis and characterisation of nano SiO_2/TiO_2 composite for insulation application," *Malaysian Journal of Chemical Engineering and Technology*, vol. 4, no. 2, pp. 155-166, 2021, https://doi.org/10.24191/mjcet.v4i2.14972

[29] K. De Witte *et al.*, "Influence of the synthesis parameters of TiO_2-SBA-15 materials on the adsorption and photodegradation of rhodamine-6G," *Microporous and Mesoporous Materials*, vol. 110, no. 1, 2008, https://doi.org/10.1016/j.micromeso.2007.09.035

[30] Y. Cheng, F. Luo, Y. Jiang, F. Li, and C. Wei, "The effect of calcination temperature on the structure and activity of TiO_2/SiO_2 composite catalysts derived from titanium sulfate and fly ash acid sludge," *Colloids and Surfaces A: Physicochemical and Engineering Aspects*, vol. 554, 2018, https://doi.org/10.1016/j.colsurfa.2018.06.032

[31] T. Cetinkaya, L. Neuwirthová, K. M. Kutláková, V. Tomášek, and H. Akbulut, "Synthesis of nanostructured TiO_2/SiO_2 as an effective photocatalyst for degradation of acid orange," *Applied Surface Science*, vol. 279, 2013, https://doi.org/10.1016/j.apsusc.2013.04.121

[32] J. Li *et al.*, "Advances in Z-scheme semiconductor photocatalysts for the photoelectrochemical applications: A review," *Carbon Energy*, 2022. https://doi.org/10.1002/cey2.179

[33] D. Wang *et al.*, "Engineering and modeling perspectives on photocatalytic reactors for water treatment," *water research*, 2021. https://doi.org/10.1016/j.watres.2021.117421

[34] R. Vijayalakshmi and V. Rajendran, "Synthesis and characterization of nano-TiO_2 via different methods," *Scholar Research Library*, vol. 4, no. 2, 2012.

[35] L. Sikong, J. Damchan, K. Kooptarnond, and S. Niyomwas, "Effect of doped SiO_2 and calcinations temperature on phase transformation of TiO_2 photocatalyst prepared by sol-gel method," *Songklanakarin Journal of Science and Technology*, vol. 30, no. 3, 2008.

[36] C. G. Joseph, Y. H. Taufiq-Yap, G. Li Puma, K. Sanmugam, and K. S. Quek, "Photocatalytic degradation of cationic dye simulated wastewater using four radiation sources, UVA, UVB, UVC and solar lamp of identical power output," *Desalination Water Treatment*, vol. 57, no. 17, 2016, https://doi.org/10.1080/19443994.2015.1063463

[37] M. Zarei, A. R. Khataee, R. Ordikhani-Seyedlar, and M. Fathinia, "Photoelectro-Fenton combined with photocatalytic process for degradation of an azo dye using supported TiO_2 nanoparticles and carbon nanotube cathode: Neural network modeling," *Electrochimica Acta*, vol. 55, no. 24, 2010, https://doi.org/10.1016/j.electacta.2010.07.050

[38] M. Khraisheh, L. Wu, A. H. Al-Muhtaseb, A. B. Albadarin, and G. M. Walker, "Phenol degradation by powdered metal ion modified titanium dioxide photocatalysts," *Chemical Engineering Journal*, vol. 213, 2012, https://doi.org/10.1016/j.cej.2012.09.108

[39] A. N. Kassob and A. H. Abbar, "Treatment of Petroleum Refinery Wastewater by Graphite–Graphite Electro Fenton System Using Batch Recirculation Electrochemical Reactor," *Journal of Ecological Engineering*, vol. 23, no. 10, 2022, https://doi.org/10.12911/22998993/152524

[40] M. M. Jiad and A. H. Abbar, "Efficient wastewater treatment in petroleum refineries: Hybrid electro-fenton and photocatalysis (UV/ZnO) process," *Chemical Engineering Research and Design*, vol. 200, 2023, https://doi.org/10.1016/j.cherd.2023.10.050

[41] W. Rice, R. B. Baird, A. D. Eaton, and L. S. Clesceri, "Standard methods for the examination of water and wastewater," *Washington, DC American Public Health Association American Water Works*, 2012.

[42] T. N. S. Ho, T. T. Nguyen, T. H. T. Pham, M. T. Ngo, and M. V. Le, "Photocatalytic degradation of phenol in aqueous solutions using TiO_2/SiO_2 composite," *Chemical Engineering Transactions*, vol. 78, 2020, https://doi.org/10.3303/CET2078072

[43] S. Yohi, C. M. Wu, and R. T. Koodali, "A Kinetic Study of Photocatalytic Degradation of Phenol over Titania–Silica Mixed Oxide Materials under UV Illumination," *Catalysts*, vol. 12, no. 2, 2022, https://doi.org/10.3390/catal12020193

[44] T. Degen, M. Sadki, E. Bron, U. König, and G. Nénert, "The high score suite," in *Powder Diffraction*, 2014. https://doi.org/10.1017/S0885715614000840

[45] M. A. Gatou, E. Fiorentis, N. Lagopati, and E. A. Pavlatou, "Photodegradation of Rhodamine B and Phenol Using TiO_2/SiO_2 Composite Nanoparticles: A Comparative Study," *Water (Switzerland)*, vol. 15, no. 15, 2023, https://doi.org/10.3390/w15152773

[46] A. Duran, C. Serna, V. Fornes, and J. M. Fernandez Navarro, "Structural considerations about SiO_2 glasses prepared by sol-gel," *Journal of Non-Crystalline Solids*, vol. 82, no. 1–3, 1986, https://doi.org/10.1016/0022-3093(86)90112-2

[47] Gobara, R. El-Salamony, D. Mohamed, M. Mishrif, Y. Moustafa, and T. Gendy, "Use of SiO_2-TiO_2 Nanocomposite as Photocatalyst for the Removal of Trichlorophenol: A Kinetic Study and Numerical Evaluation," *Chemistry and Materials Research*, vol. 6, no. 6, 2014.

[48] Y. D. Hou *et al.*, "N-Doped SiO_2/TiO_2 mesoporous nanoparticles with enhanced photocatalytic activity under visible-light irradiation," *Chemosphere*, vol. 72, no. 3, 2008, https://doi.org/10.1016/j.chemosphere.2008.02.035

[49] M. Bellardita *et al.*, "Photocatalytic activity of TiO_2/SiO_2 systems," *Journal of Hazardous Materials*, vol. 174, no. 1–3, 2010, https://doi.org/10.1016/j.jhazmat.2009.09.108

[50] A. Siddiqa, S. Sabir, S. T. Hussain, and B. Muhammad, "Highly active mesoporous SiO_2-TiO_2 based nanocomposites for photocatalytic degradation of textile dyes and phenol," *European Journal of Chemistry*, vol. 4, no. 4, 2013, https://doi.org/10.5155/eurjchem.4.4.388-395.826

[51] R. Khataee, M. Zarei, and R. Ordikhani-Seyedlar, "Heterogeneous photocatalysis of a dye solution using supported TiO_2 nanoparticles combined with homogeneous photoelectrochemical process: Molecular degradation products," *Journal of Molecular Catalysis A: Chemical*, vol. 338, no. 1–2, 2011, https://doi.org/10.1016/j.molcata.2011.01.028

[52] L. Cui, Y. Song, F. Wang, Y. Sheng, and H. Zou, "Electrospinning synthesis of SiO_2-TiO_2 hybrid nanofibers with large surface area and excellent photocatalytic activity," *Applied Surface Science*, vol. 488, 2019, https://doi.org/10.1016/j.apsusc.2019.05.151

[53] Y. Hendrix, A. Lazaro, Q. Yu, and J. Brouwers, "Titania-Silica Composites: A Review on the Photocatalytic Activity and Synthesis Methods," *World Journal of Nano Science and Engineering*, vol. 05, no. 04, 2015, https://doi.org/10.4236/wjnse.2015.54018

[54] R. Sellappan, "Mechanisms of Enhanced Activity of Model TiO_2/Carbon and TiO_2/Metal Nanocomposite Photocatalysts," *Thesis for the Degree of Doctor of Philosophy*, 2013.

[55] Z. Guo *et al.*, "Photodegradation of organic micropollutants in aquatic environment: Importance, factors and processes," *water research*, 2023. https://doi.org/10.1016/j.watres.2022.118236

[56] A. R. A. Giwa, I. A. Bello, A. B. Olabintan, O. S. Bello, and T. A. Saleh, "Kinetic and thermodynamic studies of fenton oxidative decolorization of methylene blue," *Heliyon*, vol. 6, no. 8, 2020, https://doi.org/10.1016/j.heliyon.2020.e04454

[57] Z. H. Jabbar, S. E. Ebrahim, and S. H. Ammar, "Supported heterogeneous nanocomposites ($SiO_2/Fe_3O_4/Ag_2WO_4$) for visible-light-driven photocatalytic disinfection against E. coli," *Material Science in Semiconductor Processing*, vol. 141, 2022, https://doi.org/10.1016/j.mssp.2021.106427

[58] N. M. Bahadur *et al.*, "Ultrasonic-Assisted Synthesis, Characterization, and Photocatalytic Application of SiO_2@TiO_2 Core-Shell Nanocomposite Particles," *Journal of Nanomaterials*, vol. 2019, 2019, https://doi.org/10.1155/2019/6368789

[59] R. C. Ngullie, S. O. Alaswad, K. Bhuvaneswari, P. Shanmugam, T. Pazhanivel, and P. Arunachalam, "Synthesis and characterization of efficient ZnO/g-C_3N_4 nanocomposites photocatalyst for photocatalytic degradation of methylene blue," *Coatings*, vol. 10, no. 5, 2020, https://doi.org/10.3390/COATINGS10050500

[60] E. K. Tetteh, D. B. Naidoo, and S. Rathilal, "Optimization of photo-catalytic degradation of oil refinery wastewater using Box-Behnken design," *Environmental Engineering Research*, vol. 24, no. 4, 2019, https://doi.org/10.4491/eer.2018.216

[61] M. Al-Tameemi, K. A. Sukkar, A. H. Abbar, and Z. K. Kuraimid, "Optimization of photocatalytic process with SnO_2 catalyst for COD reduction from petroleum refinery wastewater using a slurry bubble photoreactor," *Case Studies in Chemical and Environmental Engineering*, vol. 9, 2024, https://doi.org/10.1016/j.cscee.2024.100687

[62] E. K. Tetteh, S. Rathilal, and D. B. Naidoo, "Photocatalytic degradation of oily waste and phenol from a local South Africa oil refinery wastewater using response methodology," *Scientific Reports*, vol. 10, no. 1, p. 8850, 2020, https://doi.org/10.1038/s41598-020-65480-5

[63] Saien and F. Shahrezaei, "Organic pollutants removal from petroleum refinery wastewater with nanotitania photocatalyst and UV light emission," *International Journal of Photoenergy*, vol. 2012, 2012, https://doi.org/10.1155/2012/703074

معالجة مياه الصرف الصحي الحقيقية لمصافي البترول باستخدام جسيمات نانوية من مركب أوكسيد السيليكون/ أوكسيد التيتانيوم المُحَفَّز بالاشعة فوق البنفسجية

سرمد عبدالرزاق رشيد [١،*]، ودود طاهر محمد [١]، هروادي زين الدين [٢]

١ قسم الهندسة الكيمياوية، كلية الهندسة، جامعة بغداد، بغداد ١٠٠٠١، العراق
٢ قسم عمليات الهيدروكربونات والصناعات البتروكيميائية، كلية الهندسة، جامعة بانونيا، مدينة فيسبرم، المجر

الخلاصة

تشكل مياه صرف مصافي النفط (PRW) خطراً كبيراً على صحة الإنسان والبيئة، مما دفع إلى تكثيف الجهود البحثية لإيجاد حلول فعّالة لمعالجتها. ويُعد استخدام عمليات الأكسدة المتقدمة (AOPs) من الأساليب الواعدة في إزالة الملوثات من هذه المياه. في هذا البحث، تم استخدام مفاعل ضوئي كيميائي جديد لتشغيل عملية التحفيز الضوئي بهدف إزالة الطلب الكيميائي للأوكسجين (COD) من مياه صرف مصفى الديوانية في العراق.

اعتمدت عملية المعالجة على محفزات ضوئية من TiO_2 النقي ومركب SiO_2/TiO_2، التي تم تحضيرها بتقنية السول–جيل (sol-gel) ثم تم فحصها باستخدام تقنيات XRD و FTIR و FESEM و AFM و BET و UV-DRS و PL. وقد تحققت أفضل النتائج في خفض قيمة COD وتحسين استهلاك الطاقة النوعي (EE/O) عند نسبة SiO_2/TiO_2 مقدارها ٥/٩٥% (S-5)، وجرعة محفز بلغت ٢ غم/لتر، وزمن تفاعل ٤ ساعات، واستخدام ٨ مصابيح UV-C بقدرة ٨ واط لكل منها. وقد حقق هذا الإعداد كفاءة إزالة (RE%) بلغت ٩٠% وقيمة EE/O مقدارها ٠,٥١٢ كيلوواط·ساعة/لتر.

أظهرت الاختبارات الحركية أن تدهور COD يتبع حركيات شبه المرتبة الأولى. كما بينت تجارب الكواشف الملتقِطة (scavenger tests) أن الجذر الفعال $^{\bullet}O_2^-$ هو المسؤول الرئيس عن تفكيك الملوثات. وأظهر المحفز الضوئي ثباتاً جيداً بعد خمس دورات تشغيلية، محافظاً على كفاءة إزالة تجاوزت ٨٢%.

وبشكل عام، أسهم الجمع بين المحفز الضوئي SiO_2/TiO_2 والتصميم الجديد للمفاعل في تحسين معالجة مياه الصرف النفطي بشكل ملحوظ، مما يوفر نهجاً فعّالاً وذا جدوى اقتصادية وصديقاً للبيئة لخفض قيمة COD في مياه الصرف الصناعي لمصافي النفط.

الكلمات الدالة: إزالة COD، مركب نانوي SiO_2/TiO_2، تحلل بالتحفيز الضوئي، مياه صرف مصافي النفط PRW، المواد الملتقطة او الكانسة.